

## Upper critical field and heat capacity in the reentrant superconducting system $(\text{Lu}_{1-x}\text{Er}_x)\text{RuB}_2$

R. N. Shelton

*Ames Laboratory—U.S. Department of Energy and Department of Physics, Iowa State University, Ames, Iowa 50011*

H. E. Horng

*Department of Physics, National Taiwan Normal University, Taipei 117, Republic of China*

(Received 2 August 1985)

Low-temperature heat capacity, upper-critical-field measurements, and ac magnetic susceptibility are utilized to study the interaction between superconductivity and magnetic order in the orthorhombic compounds  $(\text{Lu}_{1-x}\text{Er}_x)\text{RuB}_2$ . Reentrant superconductivity is observed in a concentration range just below a critical value ( $x_{cr} \approx 0.5$ ), where the superconducting and magnetic phase boundaries meet. For samples with concentrations greater than  $x_{cr}$ , two magnetic transitions are observed, opening the possibility of complex magnetic states. The strength of the effective exchange field,  $H_{ex}$ , is derived from the conduction-electron—rare-earth spin-exchange interaction. Superconductivity is quenched and reentrance occurs when  $H_{ex}$  becomes comparable to the Pauli paramagnetic limiting field. Heat-capacity data for  $\text{LuRuB}_2$  yield a relatively high Debye temperature of 487 K and an electronic specific-heat coefficient of 7.05 mJ/mol K<sup>2</sup>.

### I. INTRODUCTION

Measurements of the ac magnetic susceptibility  $\chi_{ac}$  and the electrical resistance on primitive tetragonal  $\text{ErRh}_4\text{B}_4$  (Ref. 1) and Chevrel-phase  $\text{HoMo}_6\text{S}_8$  (Refs. 2 and 3) reveal a normal-to-superconducting—state transition at  $T_{c1}$  followed at lower temperatures by the onset of a magnetic transition at  $T_m$ , followed by a transition back to the normal state at  $T_{c2}$ . In these two strict ternary phases, the magnetic ions completely occupy their own unique sublattice. This reentrant superconductivity can also be induced by varying the transition metal or magnetic ion composition to alloy superconducting and magnetically ordered ternaries to form a pseudoternary solid solution such as  $\text{Ho}(\text{Rh}_{1-x}\text{Ir}_x)_4\text{B}_4$ , where reentrant superconductivity occurs between  $x=0.08$  and  $x=0.22$ , with the  $\text{Ho}^{3+}$  ions still occupying a distinct sublattice.<sup>4,5</sup> In the system  $(\text{Ho}_{1-x}\text{Lu}_x)\text{Rh}_4\text{B}_4$ ,  $\text{Ho}^{3+}$  and  $\text{Lu}^{3+}$  ions are distributed randomly on the same sublattice over the entire rare-earth concentration range, and reentrant superconductivity occurs for compositions between  $x=0.08$  and 0.72.<sup>6</sup> The magnetic rare-earth (RE) ions are distributed in a periodic array throughout the lattice, and the magnetic order is long range in nature.

Recently, new superconducting ternary borides  $MTB_2$  ( $M=\text{Sc}, \text{Y}, \text{Lu}$  and  $T=\text{Ru}, \text{Os}$ ) with superconducting transition temperatures from 1.3 K for  $\text{ScOsB}_2$  to 10.0 K for  $\text{LuRuB}_2$  have been reported with an orthorhombic structure.<sup>7,8</sup> The isostructural, magnetically ordered compounds with  $M=\text{Tb}, \text{Dy}, \text{Ho}, \text{Er},$  or  $\text{Tm}$  have magnetic transition temperatures between 2 and 46 K. The suitably high superconducting transition temperature of 10.0 K for  $\text{LuRuB}_2$  provides a good opportunity for a systematic study of the questions of reentrant and coexistent superconductivity. One of the isomorphous pseudoternary systems,  $(\text{Tm}_{1-x}\text{Lu}_x)\text{RuB}_2$ , has been reported with reentrant

superconductivity occurring between rare-earth concentrations  $x=0.52$  and 0.68.<sup>9</sup> The absence of coexistence between superconductivity and long-range magnetic order in this system suggested a ferromagneticlike nature of the magnetic state.<sup>9</sup> Similar to the 1:4:4 composition ratio borides, boron pairs also appear in this structure. With the lower transition-metal concentration, the  $\text{LuRuB}_2$ -type structure possesses some crystallographic features which are not present in  $MT_4B_4$  structures, namely, (i) the absence of transition-metal clusters, (ii) the relatively long distance between Ru atoms (3.03 Å), and (iii) the short (3.10 Å) Lu—Lu intraplanar bonds. This short RE-RE distance and the possibility for direct coupling between rare-earth atoms motivated this investigation into the strength of the pair breaking interaction in these materials. Additionally,  $\text{ErRuB}_2$  was found in this work to exhibit two distinct magnetic ordering temperatures, 10.0 and 5.3 K, rather than the previously reported single transition 5.21 K.<sup>7</sup> This difference attracted our attention to the relation between two transitions and the effect of the  $\text{Er}^{3+}$  ion in the  $\text{LuRuB}_2$  structure; therefore, the pseudoternary system  $(\text{Lu}_{1-x}\text{Er}_x)\text{RuB}_2$  was studied in its entirety.

To further characterize these materials, resistivity data, upper-critical-field determination, and heat-capacity measurements are included in order to clearly define the electronic properties. Various superconducting- and normal-state parameters are derived.

### II. EXPERIMENTAL DETAILS

All samples were synthesized in an identical manner. The rare-earth elements were arc-melted together to form a master ingot of  $\text{LuEr}$  as a starting material for pseudoternaries  $(\text{Lu}_{1-x}\text{Er}_x)\text{RuB}_2$ . After a stoichiometric amount of boron was arc-melted into a ruthenium ingot,

the appropriate ratio of starting material (LuEr), pure rare-earth element (either Lu or Er), and  $\text{RuB}_2$  was fixed by arc-melting them into one ingot. This final product was melted several times to promote homogeneity. Finally, the samples were sealed in a Ta tube with an argon atmosphere and annealed according to the schedule: two days at  $1250^\circ\text{C}$ , from two to three weeks at  $1000^\circ\text{C}$ , followed by a quench in water to room temperature.

Powder x-ray data showed the annealed sample of  $\text{ErRuB}_2$  had an extremely small amount of unidentified ternary phase (approximately 5%). All other samples were single phase as determined by powder x-ray data. The phase boundaries between the paramagnetic, superconducting, and magnetically ordered phases in this pseudoternary system have been determined by ac magnetic-susceptibility measurements down to 1.1 K. The room-temperature resistivity for  $\text{LuRuB}_2$  was determined by a dc method using four leads attached to a rectangular-shaped sample having dimensions of approximately  $0.5 \times 1.5 \times 0.7 \text{ mm}^3$ . The slope of the  $V$ - $I$  curve was used to determine the resistance. Because of slight anisotropy in the resistance of these samples, perhaps caused by preferred crystallite orientation when quenching samples in the arc furnace, a correction to the van der Pauw method<sup>10</sup> was made based on the report of Montgomery.<sup>11</sup> The heat-capacity data were obtained between 0.6 and 26 K for a 4-g  $\text{LuRuB}_2$  bulk sample.

### III. RESULTS AND DISCUSSION

#### A. Crystallographic and electronic properties

The ac magnetic susceptibility versus temperature for three selected samples is shown in Fig. 1. The sample with rare-earth concentration  $x=0$  shows a simple superconducting transition, while the sample with  $x=0.47$  exhibits the reentrant behavior. For the susceptibility data, we define the critical temperature,  $T_c$  or  $T_{c1}$ , as the midpoint of the transition into the superconducting state, while  $T_{c2}$  is the temperature at which the superconducting state is completely destroyed. Two peaks due to magnetic order appear at 10.0 and 5.3 K and are defined as

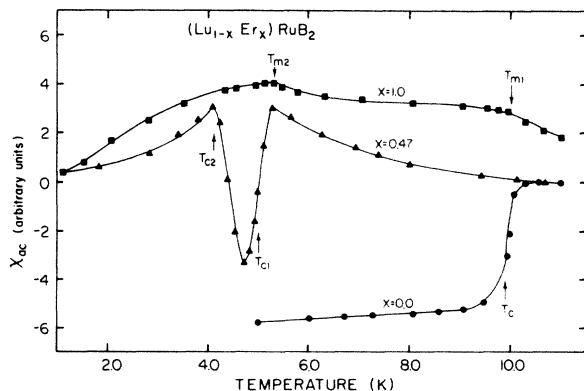


FIG. 1. ac magnetic susceptibility versus temperature for three compounds in the system  $(\text{Lu}_{1-x}\text{Er}_x)\text{RuB}_2$ . Critical temperatures for (●) superconductivity ( $T_c, T_{c1}$ ), (■) magnetic order ( $T_{m1}, T_{m2}$ ), and (▲) reentrant behavior ( $T_{c2}$ ) are noted.

$T_{m1}$  and  $T_{m2}$ , respectively, for  $\text{ErRuB}_2$ .

The low-temperature phase diagram for the pseudoternary system is completed by ac magnetic-susceptibility measurements and represented in Fig. 2. This critical temperature versus rare-earth concentration plot shows the sample  $\text{LuRuB}_2$  with  $T_c \approx 9.9 \text{ K}$  having the highest superconducting transition temperature for any material with an orthorhombic structure. With increasing erbium concentration, the depression of  $T_c$  is  $dT_c/dx = -0.11 \text{ K/at.}\% \text{ Er}^{3+}$ . A similar rate was observed for  $\text{Tm}^{3+}$  ions in the  $(\text{Tm}_{1-x}\text{Lu}_x)\text{RuB}_2$  system.<sup>9</sup> It should be noted that the behavior of both magnetic transitions as a function of concentration is identical; that is, we observe two parallel sets of magnetic transitions from  $T_{m1} = 10.0 \text{ K}$  and  $T_{m2} = 5.3 \text{ K}$  for  $\text{ErRuB}_2$  with the decreasing rate  $dT_m/dx = -0.10 \text{ K/at.}\% \text{ Lu}$ . This is the first report of double magnetic transitions in a reentrant superconducting system. The region between the extrapolation curve of the first set of magnetically ordered transitions at the Er-rich side, expressed by the dashed line in Fig. 2, and the  $T_{c2}$  curve is possibly a region in which the superconducting state and a complex magnetic state may coexist as in  $\text{ErRh}_4\text{B}_4$  (Ref. 12) and  $\text{HoMo}_6\text{S}_8$  (Ref. 13).

The initial depression  $dT_c/dn$  near  $\text{LuRuB}_2$  caused by the magnetic  $\text{Er}^{3+}$  ions of atomic concentration  $n$  can be used to estimate the exchange-coupling constant  $N(E_F)\Gamma^2$  from the Abrikosov-Gorkov expression<sup>14</sup>

$$(dT_c/dn)_{n \rightarrow 0} = -\pi^2 N(E_F) \Gamma^2 (g_J - 1)^2 J(J+1) / 2k_B, \quad (1)$$

where  $N(E_F)$  is the density of states at the Fermi energy,  $\Gamma$  is the exchange-coupling parameter between the conduction electrons and  $\text{Er}^{3+}$  local moments,  $g_J$  is the Lande  $g$  factor for the total angular momentum  $J$  of the  $\text{Er}^{3+}$  ions and forms the de Gennes factor  $(g_J - 1)^2 J(J+1)$ , and  $k_B$  is the Boltzmann constant.

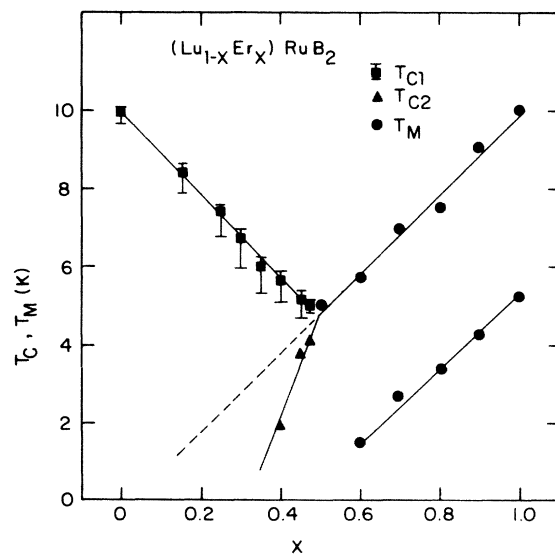


FIG. 2. Low-temperature phase diagram for the system  $(\text{Lu}_{1-x}\text{Er}_x)\text{RuB}_2$ . Superconducting ( $T_{c1}$ ), magnetic ( $T_m$ ), and reentrant ( $T_{c2}$ ) temperatures are noted. Error bars on  $T_{c1}$  represent 10–90% transition widths.

Using  $4(dT_c/dx)_{x \rightarrow 0} = (dT_c/dn)_{n \rightarrow 0}$ ,  $g_J = 1.20$  for the  $\text{Er}^{3+}$  ion and our experimental value of  $(dT_c/dx)_{x \rightarrow 0} = -0.11$  K/at. %  $\text{Er}^{3+}$  yields a value of  $2.88 \times 10^{-4}$  (eV atom states)/spin-direction for the coupling constant  $\Gamma^2 N(E_F)$ . This value is about 1.7 times larger than that obtained for the  $(\text{Ho}_{1-x}\text{Lu}_x)\text{Rh}_4\text{B}_4$  (Ref. 6) system and 2.5 times smaller than that reported for  $(\text{Tm}_{1-x}\text{Lu}_x)\text{RuB}_2$  (Ref. 9) pseudoternaries. For each of these systems, the analysis used the full value of  $J$  from the Hund's-rule ground state of the rare-earth ion. Crystalline electric field effects could result in a different  $J$  at low temperature.

The smooth linear behavior of the lattice parameters and unit-cell volume is shown in Fig. 3. This regular dependence of crystallographic parameters on rare-earth concentration is similar to behavior reported for other pseudoternary superconducting-magnetic systems.<sup>15,16</sup> The distinct and abrupt changes from simple superconductivity to reentrant superconductivity to long-range magnetic order are not reflected in these crystallographic quantities.

The resistivity as a function of temperature for four samples in this system is presented in Fig. 4. Note that the compounds with higher  $T_c$  exhibit a more pronounced negative curvature in the resistivity. This negative curvature has been observed in high- $T_c$  A15 compounds.<sup>17</sup> One common test for the purity of a metal is that it has a

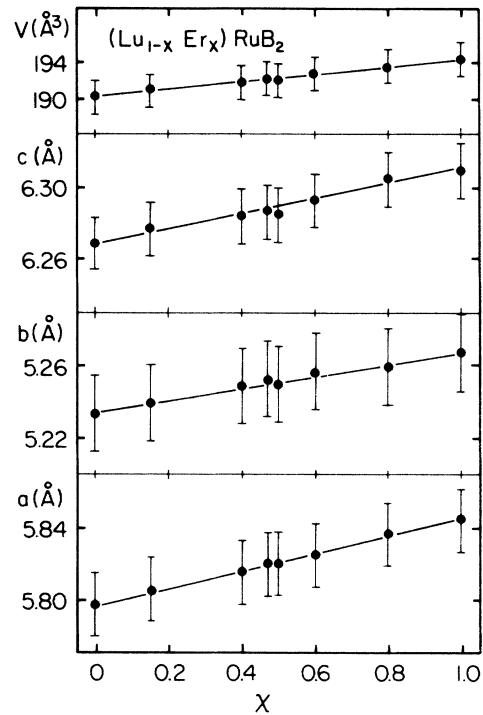


FIG. 3. Lattice parameters and unit-cell volume for compounds in the orthorhombic series  $(\text{Lu}_{1-x}\text{Er}_x)\text{RuB}_2$ .

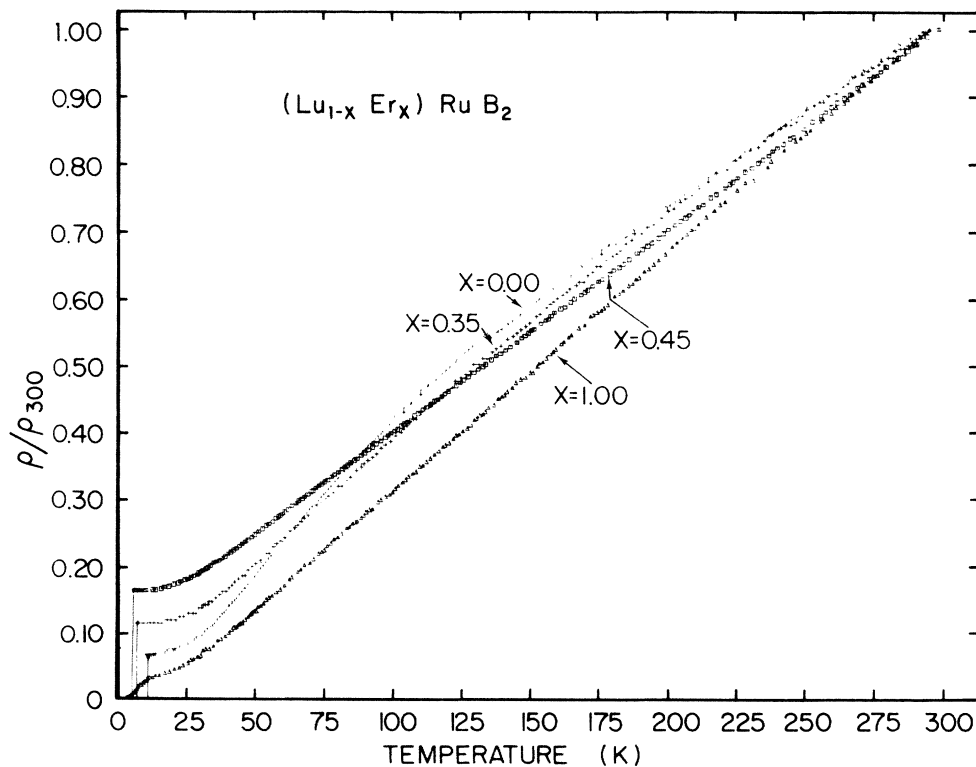


FIG. 4. Electrical resistivity normalized to the value at room temperature as a function of temperature for four compounds in the system  $(\text{Lu}_{1-x}\text{Er}_x)\text{RuB}_2$ .

TABLE I. Summary of experimental data for superconducting samples in the  $(\text{Lu}_{1-x}\text{Er}_x)\text{RuB}_2$  system.

Sample	$\chi_{ac}$ data		Resistivity data			$-\frac{dH_{c2}}{dT}$ (kOe/K)	$T_c$	$\rho_{res}$ ( $\mu\Omega$ cm)	$\gamma$ (mJ/mol K <sup>2</sup> )	$N^*(E_F)$ $\frac{\text{states}}{\text{eV atom spin}}$
	$T_{c1}$ (K) <sup>a</sup>	$T_{c2}$ (K)	$T_{c1}$ (K) <sup>a</sup>	$T_{c2}$ (K)	$T_c$ (K)					
$\text{LuRuB}_2$	10.10–9.70		10.72–10.44			7.5	55	8.7	0.46	
$(\text{Lu}_{0.85}\text{Er}_{0.15})\text{RuB}_2$	8.50–7.75		9.21–8.51			5.8	44	8.4	0.44	
$(\text{Lu}_{0.65}\text{Er}_{0.35})\text{RuB}_2$	6.28–5.30		7.03–6.85			2.5	22	7.3	0.42	
$(\text{Lu}_{0.60}\text{Er}_{0.40})\text{RuB}_2$	5.88–5.10	1.91	6.42–6.17	~2		2.0	19	6.7	0.36	
$(\text{Lu}_{0.55}\text{Er}_{0.45})\text{RuB}_2$	5.33–4.83	3.75	5.57–4.95	3.87		0.90	15	3.6	0.19	

<sup>a</sup>Values represent 10–90% transition widths.

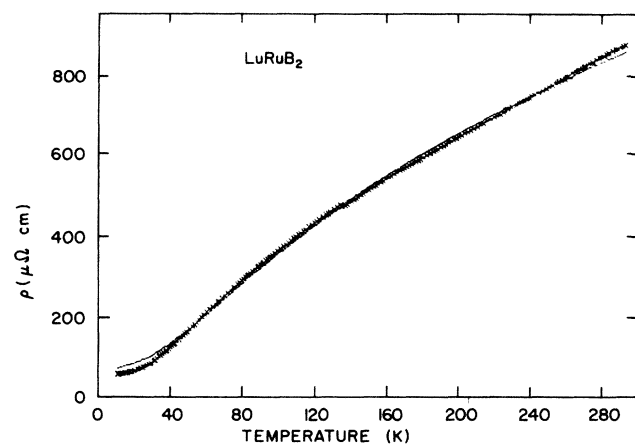
low residual resistivity or equivalently a high residual resistance ratio (RRR). On close inspection of these four relative resistivity curves, one notes that the lowest RRR occurs for the  $x=0.45$  sample. This indicates the increased scattering of conduction electrons due to the disorder on the rare-earth sublattice sites. RRR values for our samples vary from roughly 6 to 14 over the concentration range  $x=0.0$  to  $x=0.45$ . The small bump in relative resistance for the  $\text{LuRuB}_2$  sample at  $\sim 130$  K is probably caused by an error in measurement and was not reproducible. Examining the resistivity data for the magnetically ordered sample  $\text{ErRuB}_2$ , one observes that the curvature disappears in this sample. A drop in resistance begins at  $T_{m1}=10$  K, indicative of the decrease in the spin-disorder scattering occurring below the first magnetic ordering temperature. Any feature in the resistivity at  $T_{m2}$  is difficult to distinguish due to the small value of  $\rho$  at this low temperature.

For isotropic materials, the resistivity can be obtained from the resistance by applying the van der Pauw method.<sup>10</sup> Due to preferred orientation of grains which occurred in the synthesis, we use the method of Montgomery<sup>11</sup> to correct the results, assuming grain-boundary scattering is the primary factor causing the anisotropy. From a sample in the shape of a rectangular parallelepiped, a value of  $866 \mu\Omega$  cm is calculated as the room-temperature resistivity of  $\text{LuRuB}_2$ . Therefore, the residual resistivity  $\rho_{res}$  for this sample is  $55 \mu\Omega$  cm. The residual resistivities for five selected samples are listed in Table I.

The resistivity data for  $\text{LuRuB}_2$ , along with a best-fit curve are shown in Fig. 5. The data are fitted to an empirical formula used by Woodard and Cody<sup>18</sup> to model the resistance of  $\text{Nb}_3\text{Sn}$ :

$$\rho(T) = \rho_{res} + \rho_1 T + \rho_2 e^{-T_0/T}, \quad (2)$$

where  $\rho_{res}$  is the residual resistivity and  $\rho_1$ ,  $\rho_2$ , and  $T_0$  are fitting parameters. The second and third terms represent the high- and low-temperature limits of the occupation number of a particular phonon which assists in interband scattering according to Wilson's model of  $s$ - $d$  scattering.

FIG. 5. Resistivity versus temperature for  $\text{LuRuB}_2$ . The solid curve is a best fit to the data as detailed in the text.

The coefficients obtained from this fitting are  $1.31 \mu\Omega \text{ cm/K}$  for  $\rho_1$ ,  $651 \mu\Omega \text{ cm}$  for  $\rho_2$ , and  $136 \text{ K}$  for  $T_0$ . In the very-low-temperature range ( $T < 40 \text{ K}$ ), Eq. (2) with the calculated coefficients cannot satisfy the experimental data; however, this fit is significantly superior to any power-law fit over this wide temperature range.

Similar to  $\text{Nb}_3\text{Sn}$ , which exhibits a high superconducting transition temperature and strong negative curvature in its resistivity, the resistivity of  $\text{LuRuB}_2$  is found to obey a  $T^3$  law for  $T \lesssim 40 \text{ K}$ , indicative of  $s$ - $d$  phonon scattering at low temperature. The fitting equation is given for very-low-temperature data ( $T_c$  to  $\sim 40 \text{ K}$ ) by

$$\rho(T) = \rho_{\text{res}} + \rho_3 T^3, \quad (3)$$

with the fitting parameter  $\rho_3 = 1.01 \times 10^{-3} \mu\Omega \text{ cm/K}^3$  as shown in Fig. 6. The inset of this figure represents the plot of  $\rho - \rho_{\text{res}}$  versus  $T^3$ . These data reveal a linear behavior and confirm that Eq. (3) is a good fit to the low-temperature resistivity of  $\text{LuRuB}_2$ . Similar results are obtained for the  $(\text{Lu}_{0.65}\text{Er}_{0.35})\text{RuB}_2$  superconducting sample with a residual resistivity of  $22.0 \mu\Omega \text{ cm}$ ,  $\rho_1 = 0.26 \mu\Omega \text{ cm/K}$ ,  $\rho_2 = 174 \mu\Omega \text{ cm}$ ,  $T_0 = 191 \text{ K}$ , and  $\rho_3 = 1.57 \times 10^{-4} \mu\Omega \text{ cm/K}^3$ . To summarize the resistivity data for the  $(\text{Lu}_{1-x}\text{Er}_x)\text{RuB}_2$  system, we find that the Woodard-Cody model for  $A15$  compounds adequately describes the resistivity data for all superconducting samples in this system within a standard deviation of 2%.

### B. The upper critical field $H_{c2}$ and density of states $N(E_F)$

The effects of an external magnetic field on the reentrant superconductivity were studied for variety of compositions. Typical traces using a temperature sweep in constant magnetic field are shown in Fig. 7 for the  $(\text{Lu}_{0.60}\text{Er}_{0.40})\text{RuB}_2$  sample. In this figure, the superconducting state exists over a 4-K-wide region in zero field. By increasing the external field, this superconducting region narrows as  $T_m$  increases and  $T_{c1}$  decreases. This

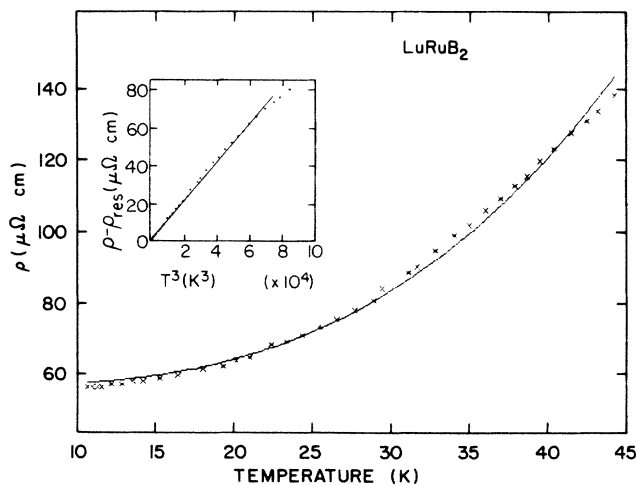


FIG. 6. Low-temperature resistivity of  $\text{LuRuB}_2$ . The inset illustrates the  $T^3$  dependence of the resistivity in this temperature range. Solid lines represent a best fit to the data as described in the text.

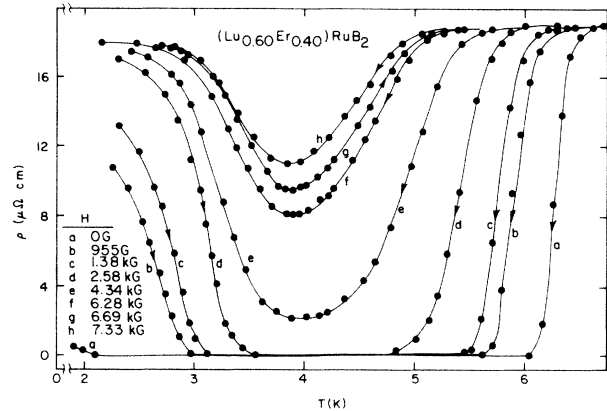


FIG. 7. Resistivity as a function of temperature in various applied magnetic fields for the reentrant superconductor  $(\text{Lu}_{0.60}\text{Er}_{0.40})\text{RuB}_2$ . Lines are drawn as a guide to the eye.

behavior of  $T_m$  in an external field implies that the low-temperature reentrant magnetic order is probably ferromagnetic. At a field between 2.6 and 4.3 kOe, the sample ceases to show a complete superconducting transition. At even higher fields, the resistive transition tends to broaden and the drop in resistivity becomes smaller. These phenomena are also seen for the  $(\text{Lu}_{0.55}\text{Er}_{0.45})\text{RuB}_2$  sample in Fig. 8. This sample is closer to the critical composition  $x_{\text{cr}} = 0.50$ . For this  $x = 0.45$  sample one observes a narrower superconducting region as well as a lower critical field required to destroy superconductivity and to completely suppress the drop in resistivity.

The data in Figs. 7 and 8 as well as analogous results for the superconducting samples with  $x = 0.00, 0.15,$  and  $0.35$  in the  $(\text{Lu}_{1-x}\text{Er}_x)\text{RuB}_2$  system yield the relations between the upper critical field  $H_{c2}$  and temperature shown in Fig. 9. The maximum applied field is approximately 9 kOe in these measurements, and is not sufficient to allow the observation of the complete curve for the higher  $T_c$

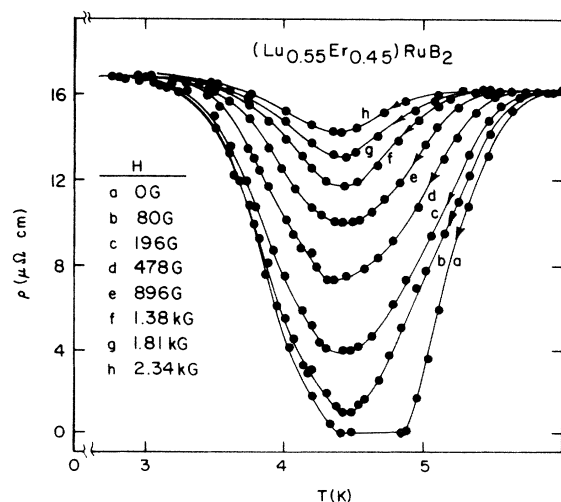


FIG. 8. Resistivity as a function of temperature in various applied magnetic fields for the reentrant superconductor  $(\text{Lu}_{0.55}\text{Er}_{0.45})\text{RuB}_2$ . Lines are drawn as a guide to the eye.

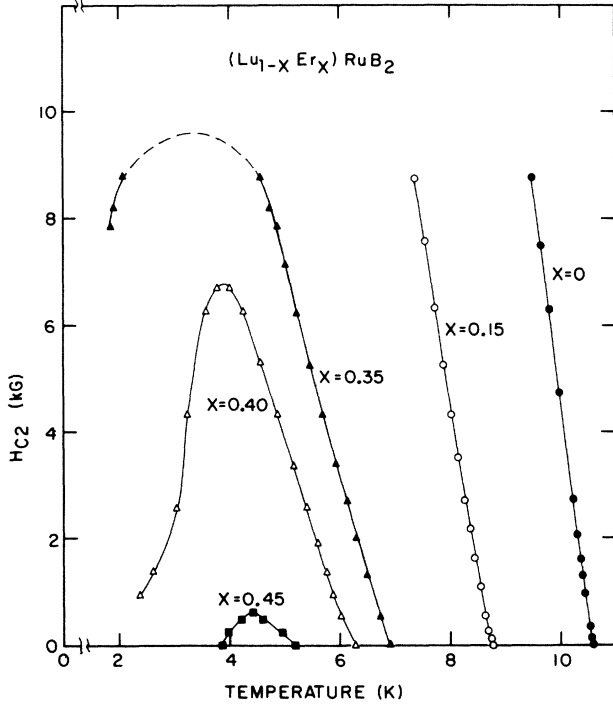


FIG. 9. Upper critical field versus temperature for five compounds in the system  $(\text{Lu}_{1-x}\text{Er}_x)\text{RuB}_2$ . Lines are drawn as a guide to the eye.

samples, for example, the samples with  $x=0.0$  and  $0.15$ . The dashed curve for the  $x=0.35$  sample in the field above 9 kOe represents the interpolation of data into this intermediate-temperature regime. Note that the reentrant behavior is evident for samples with higher  $\text{Er}^{3+}$  concentration. These measurements are consistent with data obtained from magnetic-susceptibility measurements. From this experiment, one obtains the initial slope of the upper critical field  $H_{c2}$ ,  $(dH_{c2}/dT)|_{T_c}$ , as a function of Er concentration. The linear relationship between  $(dH_{c2}/dT)|_{T_c}$  and  $x$  is shown in Fig. 10.

From the data obtained from upper-critical-field measurements, the electron-phonon-enhanced density of states  $N^*(E_F)$  can be determined by measuring  $(dH_{c2}/dT)|_{T_c}$  and the residual resistivity. The most reliable estimate for  $N^*(E_F)$  is obtained in the "dirty limit" ( $l < \xi_0$ ), where  $l$  is the electronic mean free path and  $\xi_0$  is the BCS coherence length. The BCS relationship in the dirty limit is given by<sup>19</sup>

$$-\left[\frac{dH_{c2}}{dT}\right]_{T_c} = 4.48 \times 10^4 \gamma \rho_{\text{res}}, \quad (4)$$

where  $(dH_{c2}/dT)_{T_c}$  is in Oe/K, the normal-state electronic specific-heat coefficient  $\gamma$  is in  $\text{erg cm}^{-3}\text{K}^{-2}$ , and  $\rho_{\text{res}}$  is in  $\Omega \text{ cm}$ . Measurements of  $(dH_{c2}/dT)|_{T_c}$  and  $\rho_{\text{res}}$  yield an experimental determination of the quantity  $\gamma$ . The enhanced density of states at the Fermi energy is then obtained by using the formula<sup>19</sup>

$$N^*(E_F) = (2\pi^2 k_B^2/3)^{-1} \gamma = 7.97 \times 10^{30} \gamma, \quad (5)$$

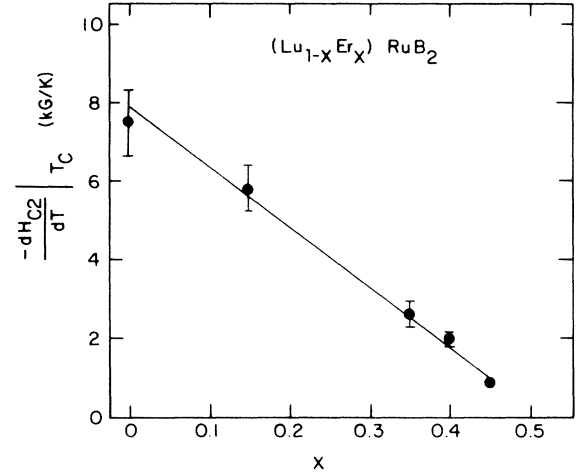


FIG. 10. Initial slope of the upper critical field as a function of Er concentration in the pseudoternary series  $(\text{Lu}_{1-x}\text{Er}_x)\text{RuB}_2$ .

where  $N^*(E_F)$  is in states/( $\text{cm}^3$  erg spin-direction) and  $\gamma$  is in  $\text{erg/cm}^3 \text{K}^2$ .

For clarity, a summary of the experimental and calculated parameters for the system  $(\text{Lu}_{1-x}\text{Er}_x)\text{RuB}_2$  is given in Table I. The transfer of units from  $\text{cm}^{-3}$  to mole is based on  $Z=4$  and the unit-cell volumes ( $\sim 190 \text{ \AA}^3$ ) for samples in this system. The calculated values  $\gamma=8.67 \text{ mJ/mol K}^2$  and  $N^*(E_F)=0.46 \text{ states/(eV atom spin-direction)}$  for  $\text{LuRuB}_2$  are smaller than  $\gamma=25.8 \text{ mJ/mol K}^2$  and  $N^*(E_F)=0.61 \text{ states/(eV atom spin-direction)}$  for  $\text{LuRh}_4\text{B}_4$ .<sup>20</sup> Our superconducting transition temperature  $T_{c1}$  and reentrant temperature  $T_{c2}$  are slightly higher as determined by resistivity measurements compared to the ac magnetic-susceptibility data. We determine the bare density of states at the Fermi energy, the electron-phonon coupling constant  $\lambda$ , and exchange coupling parameter  $\Gamma$ , with additional information from specific-heat measurements.

### C. Low-temperature specific heat

The detailed heat capacity  $C$  versus temperature  $T$  of  $\text{LuRuB}_2$  between 0.6 and 26 K is shown in Fig. 11. Heat-capacity data were taken with increasing temperature in this temperature range. The 4-g sample used for this purpose has a normal-to-superconducting transition temperature at 8.7 K determined from  $\chi_{\text{ac}}$  data. This transition temperature is lower than the  $T_c=9.9 \text{ K}$  obtained for a small sample. A possible explanation is that about 10% unidentified impurity phases yield the broader transition width in ac magnetic-susceptibility  $T_c$  determination. At  $T_c=8.9 \text{ K}$ ,  $\text{LuRuB}_2$  exhibits a specific-heat jump where it undergoes a transition from the normal to the superconducting state. This result is in good agreement with magnetic-susceptibility data obtained on the same sample. Shown in the inset of Fig. 11 is a detailed plot of  $C/T$  versus  $T^2$  from 0.6 to 26 K. A marked departure from simple Debye-type behavior above  $T_c$  is apparent.

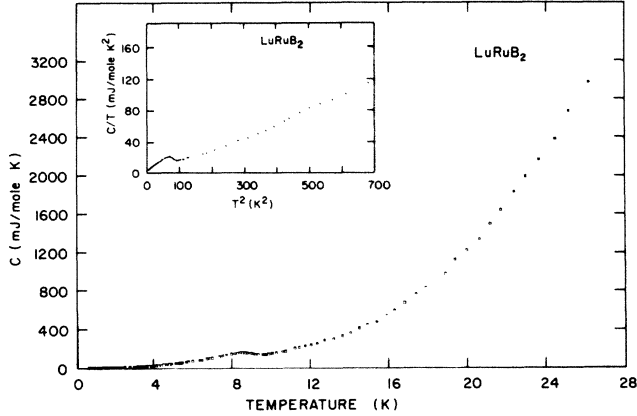


FIG. 11. Low-temperature heat capacity versus temperature for superconducting LuRuB<sub>2</sub>. The inset displays  $C/T$  vs  $T^2$ .

Since LuRuB<sub>2</sub> cannot be characterized by a Debye-type specific heat of the form  $C = \gamma T + \beta T^3$  for temperatures above  $T_c$ , an additional term  $\alpha T^5$  was used to fit the normal-state heat capacity; therefore, the expression becomes  $C = \gamma T + \beta T^3 + \alpha T^5$ . In this modified Debye model, the  $\gamma T$  term is the electron contribution to the heat capacity, while  $\beta T^3$  is the lattice contribution to the heat capacity, and the  $\alpha T^5$  term accounts for anharmonicity in the lattice. Using this expression for  $C$ , the normal-state entropy  $S$  is given by  $S = \gamma T + \frac{1}{3}\beta T^3 + \frac{1}{5}\alpha T^5$ . Plotting  $(C - S)/T^3$  versus  $T^2$  above  $T_c$  yields a linear function with an intercept of  $\frac{2}{3}\beta$  and a slope of  $\frac{4}{5}\alpha$ . Using values of  $\beta$  and  $\alpha$  obtained by a least-squares fit to this function, the normal-state heat capacity is fitted to the function  $C = \gamma T + \beta T^3 + \alpha T^5$  to obtain the additional fitting coefficient  $\gamma = 7.05$  mJ/mol K<sup>2</sup>. The calculated curve provides an excellent description of the data in the temperature range from  $T_c$  to 23 K as can be seen in Fig. 12.

In order to calculate the enhanced density of states  $N^*(E_F)$ , a convenient formula is expressed by

$$N^*(E_F) = 0.2121\gamma/N, \quad (6)$$

where the units of  $N^*(E_F)$  are states/(eV atom spin-

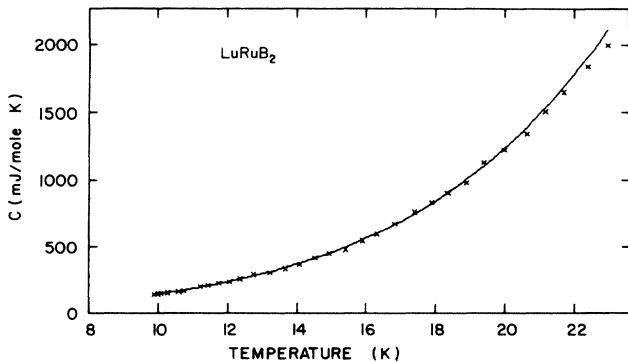


FIG. 12. Heat capacity versus temperature for LuRuB<sub>2</sub> at temperatures above the superconducting critical temperature. The solid line represents the least-squares fit to the data.

TABLE II. Superconducting and normal-state properties of LuRuB<sub>2</sub> derived from low-temperature heat-capacity data.

Parameter	Units	Value
$T_c$	K	8.9
$\Delta C$	mJ/mol K	68
$\gamma$	mJ/mol K <sup>2</sup>	7.05
$\beta$	mJ/mol K <sup>4</sup>	$6.75 \times 10^{-2}$
$\alpha$	mJ/mol K <sup>6</sup>	$1.77 \times 10^{-4}$
$\Theta_D$	K	487
$N^*(E_F)$	states/(eV atom spin)	0.37
$\lambda$		0.59
$N_b(E_F)$	states/(eV atom spin)	0.24
$\Delta C/\gamma T_c$		1.09
$2\Delta(0)/k_B T_c$		3.02
$\Gamma$	eV atom	$3.5 \times 10^{-2}$

direction), the units of  $\gamma$  are mJ/mol K<sup>2</sup>, and  $N$  is the number of atoms per formula unit. If the units of  $\beta$  are mJ/mol K<sup>4</sup>, then the Debye temperature  $\Theta_D$  in Kelvin may be calculated from

$$\Theta_D = (1.946 \times 10^6 N / \beta)^{1/3}. \quad (7)$$

From our experimental heat-capacity data and Eqs. (6) and (7), we obtain  $N^*(E_F) = 0.37$  states/(eV atom spin-direction) and  $\Theta_D = 487$  K. The jump in heat capacity at  $T_c$  yields a value of  $\Delta C/\gamma T_c = 1.09$  which is smaller than the BCS value<sup>21</sup> of 1.43. The strength of the electron-phonon interaction  $\lambda$  listed in Table II is derived from  $T_c$  using McMillan's expression<sup>22</sup> and a typical transition-metal value of 0.1 for the Coulomb pseudopotential  $\mu^*$  in the equation

$$\gamma = \frac{1.04 + \mu^* \ln(\Theta_D / 1.45 T_c)}{(1 - 0.62 \mu^*) \ln(\Theta_D / 1.45 T_c) - 1.04}. \quad (8)$$

Finally, the bare density of states  $N_b(E_F)$  is given by

$$N^*(E_F) = N_b(E_F)(1 + \lambda), \quad (9)$$

yielding a value of  $N_b(E_F) = 0.24$  states/(eV atom spin-direction) for LuRuB<sub>2</sub>. This compares a value of 0.35 states/(eV atom spin-direction) derived for LuRh<sub>4</sub>B<sub>4</sub> ( $T_c = 11.5$  K) and YRh<sub>4</sub>B<sub>4</sub> ( $T_c = 10.8$  K) from band-structure calculations.<sup>23,24</sup> Meanwhile, using the  $N_b(E_F)$  value along with  $N_b(E_F)\Gamma^2 = 2.88 \times 10^{-4}$  (eV atom states)/spin-direction, the estimated strength of the pair breaking interaction  $\Gamma$  is derived as  $3.50 \times 10^{-2}$  eV atom, which is larger than the value  $2.2 \times 10^{-2}$  eV atom for the (Lu<sub>1-x</sub>Ho<sub>x</sub>)Rh<sub>4</sub>B<sub>4</sub> (Ref. 6) system.

The energy gap at  $T=0$ ,  $\Delta(0)$ , can be deduced from the heat-capacity data  $C_s$  in the superconducting state. Taking  $C_{es}$  and  $C_l$  as the electronic and lattice contributions to the specific heat in the superconducting state, respectively, then  $C_{es} = C_s - C_l$ . In the modified Debye model described previously, the lattice part of heat capacity  $C_l$  is in the form  $C_l = \beta T^3 + \alpha T^5$ , while the electronic part near the superconducting transition can be expressed as

$$C_{es} = A_1 \exp[-(\Delta(0)/k_B T)], \quad (10)$$

where  $k_B$  is Boltzmann's constant. A least-squares fit of

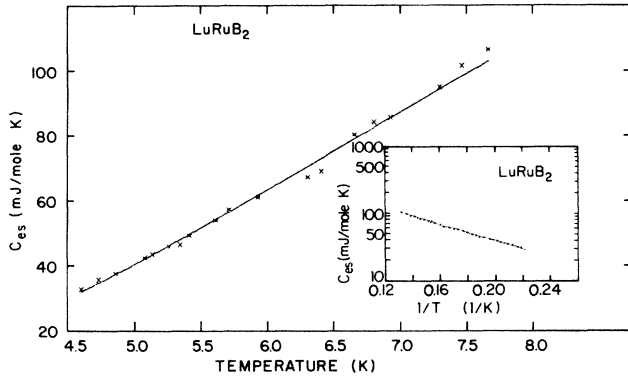


FIG. 13. Electronic heat capacity ( $C_{es}$ ) in the superconducting state of  $\text{LuRuB}_2$  as a function of temperature. The exponential dependence of  $C_{es}$  is evident in the inset where  $C_{es}$  is graphed on a log scale versus  $1/T$ . Solid lines represent the best fit to the data as described in the text.

$C_{es}$  versus temperature  $T$  is shown in Fig. 13. The fitting parameters are  $A_1 = 592$  mJ/mol K and  $\Delta(0)/k_B = 13.4$  K in the temperature range  $4.5 \leq T \leq 7.9$  K. The linearity of  $C_{es}$  plotted on a log scale versus  $1/T$  is shown in the inset of Fig. 13 and confirms the exponential dependence of  $C_{es}$ . Thus, the energy gap  $\Delta(0)$  is found to be  $1.6 \times 10^{-3}$  eV and yields the quantity  $2\Delta(0)/k_B T_c = 3.02$  which is smaller than the BCS value of 3.52. Table II provides a convenient summary of these heat-capacity data.

#### IV. DISCUSSION AND CONCLUSION

For the pure ternary  $\text{LuRuB}_2$  the low-temperature heat-capacity data are described well by a modified Debye model with a relatively high Debye temperature. The normalized jump at  $T_c$  and energy gap are both slightly smaller than the BCS values. These findings are consistent with a moderate electron-phonon coupling constant. In the pseudoternary series  $(\text{Lu}_{1-x}\text{Er}_x)\text{RuB}_2$  the occurrence of reentrant superconductivity induced by the onset of magnetic order as displayed in the concentration range  $0.35 \leq x \leq 0.50$  provides an opportunity to study the question of coexistence of superconductivity and long-range magnetic order. Ferromagnetic order is suggested by resistivity measurements at low temperature for reentrant samples under various magnetic fields. Evidence of reentrant superconductivity is present in ac magnetic-susceptibility measurements and upper-critical-field data. If one neglects the second set of magnetic transitions, the low-temperature phase diagram for the  $(\text{Lu}_{1-x}\text{Er}_x)\text{RuB}_2$  system exhibits behavior similar to other reentrant systems.

The discovery of two sets of magnetic transitions for the Er-rich compounds is different and interesting. These double transitions may signal the presence of complex

magnetic states in analogy with other superconducting-magnetic ternary systems such as the  $R_2\text{Fe}_3\text{Si}_5$  ( $R$  denotes a rare-earth element) compounds which have incommensurate magnetic structures.<sup>25</sup> A determination of the magnetic structures of  $\text{ErRuB}_2$  by neutron-diffraction experiments would be revealing.

Our analysis of critical-field and resistivity data produces different values of  $\gamma$  and  $N(E_F)$  than the fit to our experimental low-temperature heat-capacity measurements for  $\text{LuRuB}_2$  (compare Tables I and II). This 20% discrepancy may be attributed in part to the uncertainty in determining an absolute value for the residual resistivity  $\rho_{res}$ , which is an important quantity for calculating  $\gamma$  from critical-field data [Eq. (4)]. The values of  $\gamma$  and  $N(E_F)$  obtained from low-temperature heat-capacity experiments should be considered more accurate for  $\text{LuRuB}_2$ . The critical-field measurements are important because they show the linear decrease of  $N(E_F)$  as the Er concentration increases across the pseudoternary series  $(\text{Lu}_{1-x}\text{Er}_x)\text{RuB}_2$ .

In ternary superconductors containing a regular sublattice of magnetic rare-earth ions, the effective exchange field  $H_{ex}$  may be derived from the conduction-electron-rare-earth spin-exchange interaction term in the Hamiltonian

$$\mathcal{H} = -\Gamma(g_J - 1)\mathbf{J} \cdot \mathbf{s} = \mathbf{H}_{ex} \cdot \boldsymbol{\mu}_{eff}, \quad (11)$$

where  $\mathbf{H}_{ex} = \Gamma(g_J - 1)\mathbf{J}/g\mu_B$ ,  $\boldsymbol{\mu}_{eff} = g\mu_B \mathbf{s}$  is the effective moment, and  $g$  is the gyromagnetic ratio. If  $H_{ex}$  exceeds  $H_p$ , the Pauli paramagnetic limiting magnetic field  $H_p = \Delta(0)/(2\mu_B)^{1/2} = 18.4 T_c$  (kOe), a first-order transition from the superconducting to the normal state would be expected. For the  $(\text{Lu}_{1-x}\text{Er}_x)\text{RuB}_2$  system, these fields, due to the magnetic  $\text{Er}^{3+}$  ions, can be estimated from our experimental data to be  $H_{ex} \cong 480$  kOe and  $H_p \cong 180$  kOe. In this pseudoternary system, the effective  $H_{ex}$  should be modified by multiplying by the fraction of  $\text{Er}^{3+}$  ions present when reentrance is first observed. With  $x = 0.38$ , the result  $H_{ex} \cong 180$  kOe =  $H_p$  gives an excellent explanation for the reentrant phenomena starting from  $x \cong 0.4$ . We conclude that this exchange mechanism is responsible for the destruction of superconductivity in these alloys.

#### ACKNOWLEDGMENTS

Ames Laboratory is operated for the U.S. Department of Energy by Iowa State University under Contract No. W-7405-Eng-82. Research at Ames was supported by the Director for Energy Research, Office of Basic Energy Sciences, Grant No. WPAS-KC-02-02-02. Work at Taipei was supported by the National Science Council, Republic of China.

- <sup>1</sup>H. R. Ott, W. A. Fertig, D. C. Johnston, M. B. Maple, and B. T. Matthias, *J. Low Temp. Phys.* **33**, 159 (1978).
- <sup>2</sup>M. Ishikawa and Ø. Fischer, *Solid State Commun.* **23**, 37 (1977).
- <sup>3</sup>L. D. Woolf, M. Tovar, H. C. Hamaker, and M. B. Maple, *Phys. Lett.* **71A**, 137 (1979).
- <sup>4</sup>H. C. Ku, F. Acker, and B. T. Matthias, *Phys. Lett.* **76A**, 399 (1980).
- <sup>5</sup>F. Acker and H. C. Ku, *Phys. Rev. B* **25**, 5692 (1982).
- <sup>6</sup>M. B. Maple, H. C. Hamaker, D. C. Johnston, H. B. Mackay, and L. D. Woolf, *J. Less-Common Met.* **62**, 251 (1978).
- <sup>7</sup>H. C. Ku and R. N. Shelton, *Mater. Res. Bull.* **15**, 1441 (1980).
- <sup>8</sup>R. N. Shelton, B. A. Karcher, D. R. Powell, R. A. Jacobson, and H. C. Ku, *Mater. Res. Bull.* **15**, 1445 (1980).
- <sup>9</sup>H. C. Ku and R. N. Shelton, *Solid State Commun.* **40**, 237 (1981).
- <sup>10</sup>L. J. van der Pauw, *Philips Res. Rep.* **13**, 1 (1958).
- <sup>11</sup>H. C. Montgomery, *J. Appl. Phys.* **42**, 297 (1971).
- <sup>12</sup>D. E. Moncton, D. B. McWhan, P. H. Schmidt, G. Shirane, W. Thomlinson, M. B. Maple, H. B. Mackay, L. D. Woolf, Z. Fisk, and D. C. Johnston, *Phys. Rev. Lett.* **45**, 2060 (1980).
- <sup>13</sup>J. W. Lynn, G. Shirane, W. Thomlinson, and R. N. Shelton, *Phys. Rev. Lett.* **46**, 368 (1981).
- <sup>14</sup>A. A. Abrikosov and L. P. Gor'kov, *Zh. Eksp. Teor. Fiz.* **39**, 1781 (1961) [*Sov. Phys.—JETP* **12**, 1243 (1961)].
- <sup>15</sup>H. E. Horng and R. N. Shelton, in *Ternary Superconductors*, edited by G. K. Shenoy, B. D. Dunlap, and F. Y. Fradin (North-Holland, New York, 1981), p. 213.
- <sup>16</sup>R. N. Shelton, H. E. Horng, A. J. Bevolo, J. W. Richardson, R. A. Jacobson, S. D. Bader, and H. C. Hamaker, *Phys. Rev. B* **27**, 6703 (1983).
- <sup>17</sup>Z. Fisk and G. W. Webb, *Phys. Rev. Lett.* **36**, 1084 (1976); H. Wiesmann, M. Gurvitch, H. Lutz, A. Ghosh, B. Schwarz, M. Strongin, P. B. Allen, and J. W. Halley, *ibid.* **38**, 782 (1977); P. B. Allen, J. C. K. Hui, W. E. Pickett, C. M. Varma, and Z. Fisk, *Solid State Commun.* **18**, 1157 (1976).
- <sup>18</sup>D. W. Woodard and G. D. Cody, *Phys. Rev.* **136**, A166 (1964).
- <sup>19</sup>T. P. Orlando, E. J. McNiff, Jr., S. Foner, and M. R. Beasley, *Phys. Rev. B* **19**, 4545 (1979).
- <sup>20</sup>L. D. Woolf, Ph.D. thesis, University of California, San Diego, 1980 (unpublished).
- <sup>21</sup>J. Bardeen, L. N. Cooper, and J. R. Schrieffer, *Phys. Rev.* **108**, 1175 (1957).
- <sup>22</sup>W. L. McMillan, *Phys. Rev.* **167**, 167 (1968).
- <sup>23</sup>T. Jarlborg, A. J. Freeman, and T. J. Watson-Yang, *Phys. Rev. Lett.* **39**, 1032 (1977).
- <sup>24</sup>A. J. Freeman and T. Jarlborg, *J. Appl. Phys.* **50**, 1876 (1979).
- <sup>25</sup>A. R. Moodenbaugh, D. E. Cox, and H. F. Braun, *Phys. Rev. B* **25**, 4702 (1982); A. R. Moodenbaugh, D. E. Cox, C. B. Vining, and C. U. Segre, *ibid.* **29**, 271 (1984).